GAIA-CLIM deliverable D4.5

Gap Analysis for Integrated Atmospheric ECV CLImate Monitoring

WP4: Assessment of reference data in global assimilation systems and characterization of key satellite data

D4.5: "Individual report on validation of satellites, 2nd version".

A Horizon 2020 project;

Grant agreement: 640276

Date: 28th February 2017

Lead Beneficiary: Met Office

Nature: Report

Dissemination level: PU

Work-package	**WP4**
Deliverable	D4.5
Nature	R
Dissemination	PU
Lead Beneficiary	Met Office
Date	28/02/2017
Status	Final
Authors	Heather Lawrence(ECMWF), Fabien Carminati (MO), William Bell (MO), Niels Bormann (ECMWF), Stuart Newman (MO), Nigel Atkinson (MO), Alan Geer (ECMWF), Stefano Migliorini (MO)
Editors	William Bell (MO), Fabien Carminati (MO), Niels Bormann (ECMWF), Nigel Atkinson (MO), Alan Geer (ECMWF)
Reviewers	Peter Thorne (NUIM), Richard Davy (NERSC), Corinne Voces (NUIM), Stephen English (ECMWF)
Contacts	heather.lawrence@ecmwf.int, william.bell@metoffice.gov.uk.
URL	http://www.gaia-clim.eu

This document has been produced in the context of the GAIA - CLIM project. The research leading to these results has received funding from the European Union's Horizon 2020 Programme under grant agreement n° 640276.

1. Introduction

The exploitation of geophysical information from Earth Observation (EO) space borne instruments depends critically on the calibration and validation of these data to a recognised standard. To date, validation of satellite instruments and derived products has been ad hoc, for example relying on satellite-to-satellite intercomparisons which lack fully traceable estimates of radiometric uncertainty. Activities within the GAIA-CLIM consortium aim to build an improved capability for satellite calibration/validation (cal/val), ultimately leading to a database of reference quality data for robust characterisation of satellite measurement uncertainties.

The framework of Numerical Weather Prediction (NWP) is attractive for assessment of satellite instrument performance, since these models ingest large volumes of observational data daily and offer comprehensive spatial and temporal sampling. However, NWP model data are not yet traceable to an absolute calibration standard. Activities within GAIA-CLIM Work Package 4 aim to develop the necessary infrastructure for the routine monitoring of reference networks such as the GCOS Reference Upper Air Network (GRUAN), linking NWP to SI standards.

Deliverable 4.5 follows up on the previous individual evaluation of validation of satellites, D4.2 and presents an evaluation of the long-term performance of the Feng Yun-3C (FY-3C) MicroWave Humidity Sounder-2 (MWHS-2) instrument, and a first assessment of the FY-3C MicroWave Radiation Imager (MWRI) instrument. This is done by comparing statistics of observation minus the short-range forecasts (O - B) from the ECMWF and Met Office systems. The aim is both to assess the quality of the observations, and to explore how short-range forecasts from NWP systems can be used as a reference for the calibration/validation of new satellite data.

This evaluation report can be found under Annex I and has also been published as ECMWF Technical Memorandum 798, “An Evaluation of FY-3C MWRI and Assessment of the long-term quality of FY-3C MWHS-2 at ECMWF and the Met Office” and is available on the ECMWF website: http://www.ecmwf.int/en/research/publications.

Annex 1

TECHNICAL MEMORANDUM

798

An Evaluation of FY-3C MWRI and Assessment of the long-term quality of FY-3C MWHS-2 at ECMWF and the Met Office

Heather Lawrence[1], Fabien Carminati[2], William Bell[2], Niels Bormann[1], Stuart Newman[2], Nigel Atkinson[2], Alan Geer[1], Keyi Chen[3] and Stefano Migliorini[2]

Research Department

[2]Met Office, Exeter, UK, [3]School of Atmospheric Sciences, Chengdu University of Information and Technology, Chengdu, China

March 2017

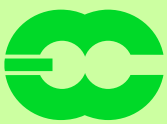

European Centre for Medium-Range Weather Forecasts
Europäisches Zentrum für mittelfristige Wettervorhersage
Centre européen pour les prévisions météorologiques à moyen terme

Series: ECMWF Technical Memoranda

A full list of ECMWF Publications can be found on our web site under:
http://www.ecmwf.int/en/research/publications

Contact: library@ecmwf.int

European Centre for Medium-Range Weather Forecasts
Shinfield Park, Reading, RG2 9AX, England

Abstract

In this report we present an evaluation of the long-term performance of the Feng Yun-3C (FY-3C) MicroWave Humidity Sounder-2 (MWHS-2) instrument, and a first assessment of the FY-3C MicroWave Radiation Imager (MWRI) instrument. This is done by comparing statistics of observation minus the short-range forecasts (O - B) from the ECMWF and Met Office systems. The aim is both to assess the quality of the observations, and to explore how short-range forecasts from NWP systems can be used as a reference for the calibration/validation of new satellite data.

Time series of mean O - B show some jumps in bias for most channels of MWHS-2 during 2016, which are consistent for both the Met Office and ECMWF statistics. These bias changes are shown to be correlated to changes in the instrument environment temperature on board the satellite. Channels 13 and 14 show large bias changes of order 2 - 3 K. However, for all other channels the bias changes are relatively small ($\sim$0.3K). In addition the standard deviation of O - B is stable over time, indicating that the MWHS-2 data are generally of good quality for most channels. This instrument continues to be assimilated at ECMWF and the Met Office, with the jumps in bias corrected by the variational bias correction schemes used at both centres.

Maps of O - B for MWRI show an ascending-descending bias of $\sim$2K for all channels, in both the ECMWF and Met Office systems. The 10.65 GHz channels have warm biases over Europe (descending only data) which are likely to be due to Radio Frequency Interference from geostationary communications satellites. Most channels of MWRI have global biases of the order -1 to -2 K for ascending data and -3 to -4 K for descending data compared to the Met Office and ECMWF short-range forecasts, and O - B statistics suggest an intersatellite bias between MWRI and AMSR-2 of approximately 4 - 6 K depending on the channel. The standard deviation of O - B is similar to AMSR-2 for most channels, however. Time series show that the ascending-descending bias for MWRI has increased in magnitude from 1 K to 2 K from 2014 to 2016. It would be useful to try to understand further the causes of the ascending-descending bias in future work since this could lead to improvements in the data for both FY-3C MWRI and future instruments.

1 Introduction

Satellite instruments sensitive to atmospheric temperature and humidity are extremely important for use in Numerical Weather Prediction (NWP) and Climate reanalysis systems. The direct assimilation of radiances from microwave and infra-red sounding and imaging instruments leads to an improved estimate of the atmospheric state, directly improving the accuracy of weather forecasts as well as the long-term monitoring of the Earth's atmosphere. When a new satellite is launched, calibration and validation of the data (cal/val) must be performed before it can be operationally assimilated into NWP and reanalysis systems. Currently, a number of techniques are employed for this, including the use of NWP short-range forecasts as a reference for assessing new data, inter-satellite comparisons using the Simultaneous Nadir Overpass (SNO) technique, and re-calibration (or bias correction) of the data by viewing a known target on Earth (e.g. Dome C, Antarctica) or in Space (e.g. the Moon). While these methods have proven to be very successful, to date none of them lead to fully traceable estimates of radiometric uncertainty.

In the GAIA-CLIM Horizon-2020 project we aim to explore further the use of NWP short-range forecasts as a reference for satellite instrument cal/val, under the activities of work package 4. To this end, a number of instruments will be assessed using the ECMWF and Met Office short-range forecasts over the lifetime of the project. Simultaneously, a method will be developed to validate NWP forecasts to reference standards using the GCOS Reference Upper Air Network (GRUAN). GRUAN sites are geographically sparse but the data have traceable uncertainty estimates, allowing us to validate the NWP fields to traceable standards. The validated NWP fields can then be used to assess new satellite data, taking advantage of their global coverage to evaluate the data over the full dynamic range of the instrument.

This report is the second in a series of assessments of new satellite data for the GAIA-CLIM project, following the report on the Advanced Microwave Scanning Radiometer 2 (AMSR-2) instrument by Newman et al. (2016). In this report we focus on the assessment of two instruments: the MicroWave Humidity Sounder -2 (MWHS-2) instrument and the MicroWave Radiation Imager (MWRI) instrument, both flown on the Chinese Feng-Yun-3C (FY-3C) polar orbiting satellite. Previously, MWHS-2 observations were assessed using observation minus background statistics by Lu et al. (2015) and by Lawrence et al. (2017) and results showed that the data were generally of good quality, with broadly similar biases to other humidity and temperature sounders. The MWHS-2 instrument is now assimilated at ECMWF and the Met Office leading to improvements in forecast accuracy (Lawrence et al., 2017). In this report we aim to build on this work by evaluating the long-term performance of the MWHS-2 instrument using observation minus background statistics.

Following an assessment of MWHS-2, we will extend the study to the MWRI instrument. MWRI is a conical-scanning microwave imager with 10 channels in the frequency range 10 GHz - 89 GHz, which have the potential to improve the estimation of total column water vapour, cloud, precipitation, ocean surface wind speed and sea-ice coverage. Similar channels can be found on the AMSR-2 instrument, assessed by Kazumori et al. (2016) and Newman et al. (2016). MWRI is part of a series of instruments which will also be flown on future Chinese polar orbiting satellites, and so it is important to evaluate the quality of the data for future satellite missions as well as FY-3C. To do so, we will compare observation minus background (O - B) statistics between ECMWF and the Met Office, and also compare statistics to AMSR-2 to further aid the identification of sources of bias.

This report is structured as follows. Firstly the two instruments, MWHS-2 and MWRI, are presented in sections 2 and 3. Secondly the calculation of observation minus background values and the selection of the data to be assessed are presented in sections 4 - 7. Finally the analysis of observation minus background statistics is presented in sections 8 and 9 and conclusions in section 10.

2 FY-3C MWHS-2 instrument

The MWHS-2 instrument has 8 channels which sample around the 118.75 GHz oxygen line, 5 channels sampling the 183 GHz water vapour line, and 2 window channels at 89 GHz and 150 GHz. Equivalent channels at 183 GHz, 89 GHz and 150 GHz are found on a number of other satellite instruments, including the Advanced Technology Microwave Sounder (ATMS) and the Microwave Humidity Sounder (MHS) instruments, but the 118 GHz channels have not been flown on a space-borne instrument before. The full list of channels for MWHS-2 with their central frequencies and horizontal resolutions is given in Table 1, with equivalent channels for ATMS and MHS also shown.

The 118 GHz and 183 GHz sounding channels of MWHS-2 provide information on temperature and humidity at different heights of the atmosphere. This is illustrated in Fig. 1, which shows the channel Jacobians (normalised by change in ln pressure). Note that Jacobians are not plotted for channels 8 and 9 since these are highly surface-sensitive and may be considered additional window channels. The 118 GHz sounding channels are primarily sensitive to atmospheric temperature, and the 183 GHz channels to atmospheric humidity. The lowest-peaking 118 GHz channel (channel 7) is sensitive to low-level humidity as well, however, due to the water vapour continuum. The 183 GHz channels and the lower peaking 118 GHz channels (channels 5 - 9) are also strongly sensitive to cloud and precipitation. The 118 GHz channels in particular are more sensitive to scattering than the traditional microwave temperature sounding channels at 53 GHz (found on the ATMS and AMSU-A instruments) due to their higher frequency. This information is useful in the all-sky assimilation carried out at ECMWF but for the pur-

Table 1: MWHS-2 and equivalent ATMS and MHS Channel frequencies and polarisation at nadir

Channel Number			Central Frequency (GHz)			Horizontal resolution (km)		
MWHS-2	ATMS	MHS	MWHS-2	ATMS	MHS	MWHS-2	ATMS	MHS
1	16	1	89 (H)	88.2 (V)	89(V)	29	32	16
2	-	-	118.75 ± 0.08 (V)	-	-	29	-	-
3	-	-	118.75 ± 0.2 (V)	-	-	29	-	-
4	-	-	118.75 ± 0.3 (V)	-	-	29	-	-
5	-	-	118.75 ± 0.8 (V)	-	-	29	-	-
6	-	-	118.75 ± 1.1 (V)	-	-	29	-	-
7	-	-	118.75 ± 2.5 (V)	-	-	29	-	-
8	-	-	118.75 ± 3.0 (V)	-	-	29	-	-
9	-	-	118.75 ± 5.0 (V)	-	-	29	-	-
10	17	2	150 (H)	165.5 (H)	157 (V)	16	16	16
11	22	3	183 ± 1.0 (V)	183 ± 1.0 (H)	183 ± 1.0 (H)	16	16	16
12	21	-	183 ± 1.8 (V)	183 ± 1.8 (H)	-	16	16	-
13	20	4	183 ± 3.0 (V)	183 ± 3.0 (H)	183 ± 3.0 (H)	16	16	16
14	19	-	183 ± 4.5 (V)	183 ± 4.5 (H)	-	16	16	-
15	18	5	183 ± 7.0 (V)	183 ± 7.0 (H)	190.31 (V)	16	16	16

pose of assessing the data quality it is important to screen for cloud and precipitation since cloud and precipitation affected data lead to a higher magnitude of departures, which tend to dominate the statistics.

Details of the design of the MWHS-2 instrument are described by Jieying et al. (2015). The instrument has 4 antennas, one each for the 118 GHz channels, the 183 GHz channels, the 89 GHz channel and the 150 GHz channel. Radiation from the Earth enters 2 apertures and is directed towards these antennas using reflectors and polar-separation grids. Pre-launch Thermal/Vacuum (T/V) tests were carried out on the MWHS-2 instrument in order to calculate the uncertainties in the calibration of each channel (both random and systematic) and determine the non-linearity corrections needed for the calibration process. Results for the 118 GHz and 89 GHz channels are presented by Jieying et al. (2015) and they show calibration uncertainties of approximately 0.3 K for most channels (118 GHz and 89 GHz) with a slightly higher uncertainty of 0.55 K for channel 2 (see Table XII of Jieying et al. (2015)).

3 FY-3C MWRI instrument

The MWRI instrument is a microwave conical-scanning imager following on the heritage of the Special Sensor Microwave Imager/Sounder (SSMI/S), Advanced Microwave Scanning Radiometer for EOS (AMSR-E) and the AMSR-2 instruments. MWRI instruments were also flown on the FY-3A and FY-3B satellites but here we evaluate the data for the FY-3C satellite only. Note that the methods applied here could be used to also assess the FY-3B MWRI instrument for potential use in reanalysis systems, however (FY-3A MWRI failed soon after launch). MWRI has 10 channels at frequencies ranging from 10.65 GHz to 89 GHz which are sensitive to total column water vapour, cloud and precipitation. Channels at the same or similar frequencies are also found on imagers aboard other polar-orbiting satellites, including the AMSR-2 instrument which was assessed in the first year of the GAIA-CLIM project (Newman et al., 2016), and the SSMI/S instruments. The main characteristics of the MWRI channels are shown in Table 2 where the equivalent values for AMSR-2 are also given for comparison[1]. Note that in this report we

[1] the information in these tables is taken from the WMO Oscar website https://www.wmo-sat.info/oscar/instruments/

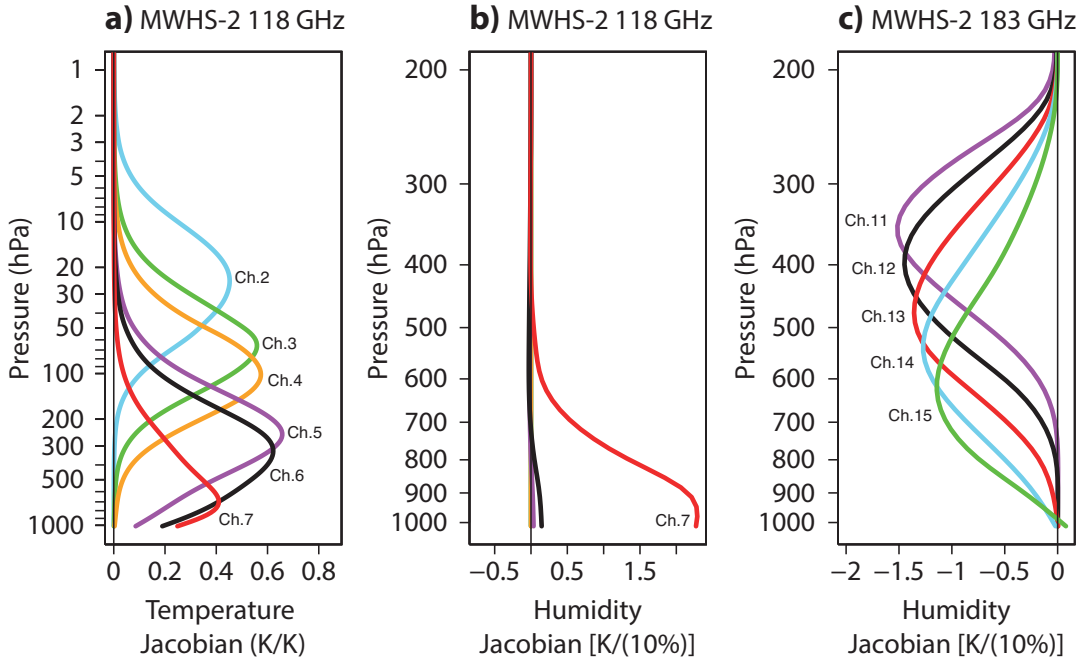

Figure 1: (a) Clear-sky Temperature Jacobians for the 118 GHz channels, (b) Clear-sky humidity Jacobians for the 118 GHz channels, and (c) Clear-sky humidity Jacobians for the 183 GHz channels. All are normalised by the model level change in the ln pressure (Δlnp)

will refer to the channels using their frequency and polarisation, as indicated in the channel name column of Table 2. For example, the 10.65 GHz H polarisation channel will be referred to as the 10H channel and the V polarisation channel 10V, etc.

Table 2: Channel frequencies, polarisations, bandwidth and field of view size for the MWRI and AMSR-2 imagers

Channel name	Central frequency (GHz)	Polarisations	Bandwidth (MHz)		IFOV	
			MWRI	AMSR-2	MWRI	AMSR-2
10V/H	10.65	V,H	180	100	51 x 85 km	24 x 42 km
19V/H	18.7	V,H	200	200	30 x 50 km	14 x 22 km
23V/H	23.8	V,H	400	400	27 x 45 km	11 x 19 km
37V/H	36.5	V,H	400	1000	18 x 30 km	7 x 12 km
89V/H	89.0	V,H	3000	3000	9 x 15 km	3 x 5 km

The MWRI instrument is designed to have a 3-point calibration method, which is a new design not found on any other conical scanning instrument. Other conical scanners such as AMSR-2 and SSMI/S have two reflectors: one for the Earth scene view and one for the cold space calibration view. In these instruments the calibration target is viewed directly by the antennas without the use of a reflector, hence not including the Earth Scene reflector in the calibration. This design has led to some strong solar-dependent biases observed in the past for the F-16 SSMI/S instrument (Bell et al., 2008) as well as the Tropical Rainfall Measuring Missions (TRMM) Microwave Imager (TMI) (Geer et al., 2010). These were diagnosed to be due to emission of the main reflector after being heated by the sun. Because the warm load calibration was not viewed through the reflector, these additional emissions were not removed in the calibration process. More recent instruments, such as AMSR-2, have not suffered similar issues however (Kazumori et al., 2016, Newman et al., 2016), following efforts by space agencies to improve the shielding of the

components of the instrument from the sun.

The 3-point calibration process for MWRI is described by Yang et al. (2011) and involves the use of 3 reflectors. The main reflector is used for the Earth-scene view, the cold-space view and the warm-load view so that any errors due to emission from the main reflector can be removed in the calibration process. In addition, there are 2 reflectors used respectively for the warm-load view and the cold-space view only. The characteristics of these reflectors can not be removed by the calibration process and so the reflectivities of these were carefully measured pre-launch (Yang et al., 2011) and the temperatures of these reflectors are also monitored on-board. Because of the geometry of MWRI and its position onboard FY-3C, when the antennas observe the warm load there is contamination from the Earth-scene via a back lobe of the main reflector and from a back lobe of the warm load. Because of this an effective warm-load temperature must be used in the calibration process, the calculation of which is outlined by Yang et al. (2011). The contributions from the Earth scene and the back lobe of the hot load are estimated to be small in comparison to the direct hot load contribution however. Yang et al. (2011) also calculated non-linearity corrections for MWRI, which were found to depend on instrument temperature. These non-linearity corrections are larger than those found for other imagers and Yang et al. (2011) concluded that the uncertainties in the non-linearity of the antennas is the largest source of calibration uncertainty for MWRI.

4 Calculating Observation Minus Background Statistics

In order to use the short-range forecasts from the ECMWF and Met Office systems as a reference for the MWHS-2 and MWRI observations, the temperature and humidity fields must first be transformed into radiance space using a radiative transfer model. This is routinely done for all satellite instruments in the ECMWF and the Met Office operational systems using the fast radiative transfer model known as RTTOV (Saunders et al., 1999). RTTOV versions 9 and 11 are used in this study, as described in sections 5 and 6. O - B values are calculated for both MWHS-2 and MWRI at the Met Office for clear-sky conditions only. However at ECMWF, they are calculated for all-sky conditions using the all-sky version of RTTOV, known as RTTOV-SCATT (Bauer et al., 2006). In this case the background values include the scattering, emission and absorption effects of cloud and precipitation as well as clear-sky radiative transfer. Surface emissivity and skin temperature fields are also required in the calculation of background radiances for surface sensitive channels. Over ocean, the emissivity is calculated from background fields using the FASTEM model at both ECMWF and the Met Office, and the skin temperature values are taken from the sea surface temperature values provided by the Met Office, for both NWP centres.

A time period for monitoring the MWHS-2 and MWRI data was jointly agreed by ECMWF and the Met Office. MWRI data were monitored offline at ECMWF and the Met Office from August 2016 to November 2016. Observation minus background statistics were calculated for 1 year of MWHS-2 data, in 2016, from the ECMWF and Met Office operational systems.

There are a number of differences in the treatment of observations at ECMWF and the Met Office, as described previously by Lu et al. (2015) and Newman et al. (2016). However, wherever possible steps were taken to minimise the effects of the differences by running different offline versions of the two models. This is described in more detail in sections 5 and 6. The similarities and differences between the approaches at the Met Office and ECMWF are also summarised in Table 3 for MWHS-2 and Table 4 for MWRI.

Table 3: Calculations of the MWHS-2 O - B values and data screening, performed at ECMWF and the Met Office. Note that an operational upgrade at ECMWF led to an increase in the horizontal resolution of the forecasts from 8 March 2016. The values given here are for the highest resolution, after this change, which is the value for the majority of the time period considered in this report.

	ECMWF	Met Office
Observation Treatment:		
Observation averaging	None	3x3 averaging
Observation thinning	Thinned to a 110 km regular grid	Thinned to an 80 km separation
Background calculations:		
Radiative transfer calculations	All-sky	Clear-sky
Radiative transfer model	RTTOV-SCATT version 11	RTTOV version 9
Hydrometeors included in calculations	Cloud liquid water, cloud ice, snow, rain	None
Ocean emissivity model	FASTEM-6	FASTEM-2
Model horizontal resolution	$\sim$ 9 km	$\sim$ 25 km
Model vertical resolution	137 levels	70 levels
Screening:		
Latitude screening	60°S $<$ latitude $<$ 60°N	60°S $<$ latitude $<$ 60°N
Land cover screening	Ocean only	Ocean only
Cloud screening	Background & observation scatter index check	Observation scatter index & cirrus cloud check
Additional screening	Cold-air outbreak screen	None

Table 4: Calculations of the MWRI and AMSR-2 O - B values and data screening, performed at ECMWF (MWRI and AMSR-2) and the Met Office (MWRI only). Note that the values given here are for the offline versions of the ECMWF and Met Office models, and are valid for most of the statistics presented in this report. There were some differences in the treatment of observations and background calculations for the statistics presented in section 9.4, as described in sections 5 and 6. Note C^b_{37} and C^o_{37} are defined in section 7.

	ECMWF	Met Office
Observation Treatment:		
Observation averaging	None	None
Observation thinning	Thinned to a 110 km regular grid	None
Background calculations:		
Radiative transfer calculations	All-sky	Clear-sky
Radiative transfer model	RTTOV-SCATT version 11	RTTOV version 11
Hydrometeors included in background calculations	Cloud liquid water, cloud ice, snow, rain	None
Hydrometeors included in C^b_{37} calculations	Cloud liquid water, cloud ice, snow, rain	Cloud liquid water, cloud ice
Ocean emissivity model	FASTEM-6	FASTEM-6
Model horizontal resolution	$\sim$ 25 km	$\sim$ 25 km
Model vertical resolution	137 levels	70 levels
Screening:		
Latitude screening	50°S $<$ latitude $<$ 50°N	50°S $<$ latitude $<$ 50°N
Land cover screening	Ocean only	Ocean only
Cloud screening	$C^b_{37} < 0.05$ and $C^o_{37} < 0.05$	$C^b_{37} < 0.05$ and $C^o_{37} < 0.05$
Additional screening	Cold-air outbreak screen	None

5 Monitoring MWHS-2 and MWRI data in the Met Office system

MWHS-2 183 GHz channels 11 - 15 are currently assimilated in the Met Office operational system, as of 15 March 2016. Observation minus background statistics are routinely calculated before assimilation for clear-sky conditions using RTTOV version 9 (RTTOV-9), which includes FASTEM version 2 (FASTEM-2). Before assimilation, the observations are averaged in a 3x3 manner. A cloud-screening is then applied which includes a scattering index check and a cirrus cloud cost test, described in more detail by Lu et al. (2015). The horizontal resolution of the background is N768 ($\sim$25 km) with 70 levels in the vertical.

MWRI data were monitored offline at the Met Office for the period considered, calculating the observation minus background values using the clear-sky background fields taken from the Met Office operational system. Observation minus background statistics were calculated in clear-sky conditions using RTTOV-9 and FASTEM-2. However, the previous study by Newman et al. (2016) showed that using different FASTEM versions for imagers leads to large bias differences which dominate the statistics. Observation minus background values were therefore also calculated for MWRI in an offline system at the Met Office using RTTOV-11 and FASTEM-6. These data were only available for 1 month however so that, while most of the results presented here were calculated using FASTEM-6, the longer time-series presented in section 9.4 is for data calculated using FASTEM-2 for the Met Office.

6 Monitoring MWHS-2 and MWRI data in the ECMWF system

MWHS-2 data have been operationally monitored at ECMWF since December 2015 and assimilated since 5 April 2016. This includes the assimilation of 118 GHz channels 2 - 7 and 183 GHz channels 11, 12 and 15. Observation minus background values are operationally calculated in all-sky conditions for all channels of MWHS-2 before assimilation and we have used these values in the following analysis. To do this RTTOV-SCATT version 11 is used to calculate the background fields in radiance space. FASTEM version 6 is used to calculate emissivity values over ocean. Before assimilation, the observations are thinned to a regular grid of approximately 110 km separation, and observation errors are calculated which are higher in regions of cloud and precipitation. At the start of 2016 the ECMWF model used a reduced linear Gaussian grid. However the grid was changed to a cubic octahedral reduced Gaussian grid on 8 March 2016, as a result of which the horizontal resolution was increased from approximately 15 km before the change to approximately 9 km after the change. For the majority of the period considered in this study, the horizontal resolution was 9 km. The ECMWF model has 137 levels in the vertical.

MWRI data are not currently monitored in the ECMWF operational system. Instead the data were monitored in an offline research assimilation experiment during the period from August 2016 to November 2016. In this experiment the treatment of MWRI observations followed the methods developed by Geer and Bauer (2010) for the assimilation of microwave imagers, which are also applied to the AMSR-2 instrument. Microwave imagers are assimilated in all-sky conditions at ECMWF, allowing the assimilation of both clear and cloud and precipitation-affected radiances. Before assimilation, the observations are first superobbed (averaged) in order to match the observation spatial scale more closely to the spatial scale of the background fields, and then thinned to a regular grid of approximately 110 km separation. Observation and background cloud amounts are also calculated from the observations and background fields of the 37 GHz channels and the average of these values is used as a predictor for the observation errors (Geer and Bauer, 2010). In the study presented in this paper we take advantage of the background and observation cloud amounts calculated in the all-sky system for MWRI, to perform a cloud screening before assessing O - B statistics (see section 7).

The offline experiment monitoring the MWRI data used the operational ECMWF model at a lower horizontal resolution, of approximately 25km, with 137 levels in the vertical (the same as operations). As with other imagers, observation minus background statistics were calculated in all-sky conditions for MWRI using RTTOV-SCATT. The data were thinned and averaged (superobbed) before calculating these statistics. However, an intial assessment of data showed that the superobbing reduced the standard deviation of O - B making it difficult to compare to data from the Met Office. We therefore ran an additional monitoring experiment for 1 month (September 2016) without superobbing for MWRI. Most statistics presented in this report are for data before superobbing, with the exception of the longer time series presented in section 9.4.

In this report, the MWRI O - B statistics are compared to values for AMSR-2 calculated in the ECMWF system. AMSR-2 data are currently assimilated in the all-sky framework at ECMWF. O - B values were calculated for AMSR-2 in all-sky conditions, and then the same cloud screening method and screening thresholds were used for both AMSR-2 and MWRI (described in section 7). The superobbing was also turned off for AMSR-2 in the offline experiment run to monitor MWRI observations, so that the O - B statistics could be directly compared between MWRI and AMSR-2.

All data were screened for cloud and precipitation in both the Met Office and ECMWF systems before calculating statistics, and a number of other screens were applied, as described in section 7.

7 Data Selection

In this study we consider only data over ocean, since the estimates of surface emissivity and skin temperature tend to be more accurate over ocean. We have also applied a latitude screen to avoid including data over sea-ice, keeping only data between 60°N and 60°S for MWHS-2 and 50°N and 50°S for MWRI. A tighter latitude screen was used for MWRI since initial maps of observation minus background showed strong biases below 50°S for the Met Office data, likely to be due to emissivity errors.

Both MWHS-2 and MWRI data were screened for cloud before analysing observation minus background statistics. We applied the same screenings as Lu et al. (2015) for MWHS-2. MWRI data were screened for cloud using the background cloud amount C^b_{37} and the observation cloud amount C^o_{37}, used previously in the assessment of AMSR-2 (Newman et al., 2016). These are calculated as follows. Firstly, the normalised polarisation difference at 37 GHz is calculated for the observations (P^o_{37}) and background (P^b_{37}), from (Geer and Bauer, 2010):

$$P^o_{37} = (T^o_v - T^o_h) \,/\, \left(T^b_{v\_clear} - T^b_{h\_clear}\right), \tag{1}$$

$$P^b_{37} = \left(T^b_v - T^b_h\right) \,/\, \left(T^b_{v\_clear} - T^b_{h\_clear}\right), \tag{2}$$

where T^o_v and T^o_h are the 37 GHz V and H polarisation observations respectively, T^b_v and T^b_h are the all-sky background brightness temperatures for these channels (calculated using RTTOV-SCATT), and T_{v_clear} and T_{h_clear} are the clear-sky background brightness temperatures for these channels (calculated using RTTOV). Note that the 37 GHz observations are used in (1) and (2) without applying a bias correction. Bias differences between the 37H and 37V observations (T^o_h and T^o_v) have a relatively small effect on P^o_{37}, however, since the denominator in (1) is of the order 80 K, so that we do not expect the bias differences to affect the cloud screening.

The observation and background cloud amounts, C^o_{37} and C^b_{37}, are calculated from P^o_{37} and P^b_{37} as follows:

$$C^o_{37} = 1 - P^o_{37}, \tag{3}$$

$$C^b_{37} = 1 - P^b_{37}, \tag{4}$$

We applied a cloud screening, keeping data which passed both thresholds (5) and (6), given below:

$$C^b_{37} < 0.05 \tag{5}$$

$$C^o_{37} < 0.05 \tag{6}$$

The threshold value of 0.05 was chosen for screening both MWRI and AMSR-2 data because it is the same threshold applied in the operational monitoring of cloud-screened data for AMSR-2 at ECMWF, as shown on the monitoring pages of the EMCWF website[2] (note that this screen is not applied in the assimilation of AMSR-2, only for monitoring the data quality). To check that this threshold was also valid for MWRI data we plotted a map of observation minus background statistics for all channels with different thresholds. A threshold of 0.05 appeared to remove the majority of cloud-affected data without screening too much clear-sky data.

The same threshold was applied to MWRI data at the Met Office. There are some differences in the calculation of C^b_{37} performed at ECMWF and the Met Office. At the Met Office only cloud liquid water and cloud ice effects are included whereas at ECMWF rain and snow effects are included as well. This leads to different values of C^b_{37} (see Fig. 2 of Newman et al. (2016) for example) so that applying this threshold keeps more Met Office data than ECMWF data. This did not appear to affect the biases or standard deviation of Met Office O - B statistics, however, most likely because these statistics are calculated using clear-sky background fields.

An additional screen was applied to ECMWF statistics to remove data where there is a known model bias; the cold-air outbreak bias. This bias affects data in high latitudes and is due to the model not producing supercooled liquid water. To screen this data we used the operational screening developed by Lonitz and Geer (2015).

8 O - B statistics for MWHS-2

A comparison of O - B statistics between ECMWF and the Met Office for the MWHS-2 instrument was previously carried out by Lu et al. (2015) for December 2015 data. Here we evaluate statistics for 2016, and compare results to the findings of Lu et al. (2015). Firstly, the mean and standard deviation for data averaged for the month of November 2016, are shown in Fig. 2. As found previously, the biases for all channels are very similar between the Met Office and ECMWF, which suggests that these biases are due in large part to calibration errors in the instrument. The standard deviation of O - B is higher for ECMWF than the Met Office, which is due to the observations being superobbed at the Met Office and not at ECMWF. There are quite large differences in the biases for channels 13 and 14 in comparison to the biases seen in 2015 (see Fig. 15 of Lu et al. (2015)): channel 13 is now 1 K warmer and channel 14

[2] www.ecmwf.int

is now 2 K warmer than December 2015. This is due to jumps and drifts observed over time, particularly in these 2 channels, and will be described further in the following. The standard deviation of O - B has not changed for most channels during this time, however, indicating that the random errors in the observations, or noise, are stable with time.

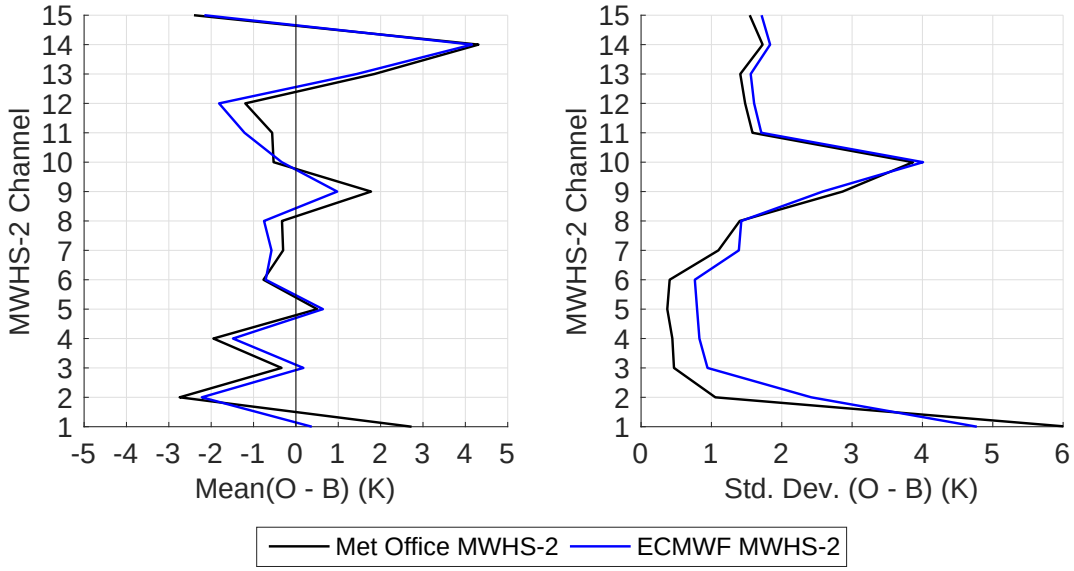

Figure 2: The mean and standard deviation of O - B for MWHS-2 in November 2016, calculated over ocean only using the ECMWF and Met Office background fields, and after cloud screening.

Over the last year a number of bias changes occurred for MWHS-2, which are consistent between ECMWF and Met Office statistics. These were found to be changes largely in the global bias values since maps of O - B were very similar before and after the bias jumps (not shown). The bias changes are illustrated in Fig. 3 for channels 2, 4, 7 (all 118 GHz), 13 and 14 (both 183 GHz). These changes in bias appear to be related to changes in the instrument environment temperature, plotted also as a time series in Fig. 3 (values taken from the direct broadcast data received at the Met Office). The Pearson's correlation coefficient between mean O - B and instrument environment temperature was calculated for all channels, for both ECMWF and Met Office statistics, and the values are given in Table 5. The linear fits are also illustrated in Fig. 4 for channels 4, 13 and 14 (ECMWF statistics).

It is interesting to note that some MWHS-2 channels are negatively correlated to the instrument temperature and some positively correlated. The correlation to instrument environment temperature is strongest for channels 13 and 14, with correlations of around -0.95 for both ECMWF and Met Office data. These two channels have the largest changes in bias, with a change of around 2 K in magnitude for channel 13 and 3 K in magnitude for channel 14, compared to bias changes of around 0.2 - 0.3 K in magnitude for other channels.

It is unclear why changes in the instrument environment temperature should lead to changes in the MWHS-2 biases, since any changes in the systematic errors of the antennas should be removed by the calibration process. One possible explanation is that a change in the non-linearity correction occurs as the instrument temperature changes, since this would not be removed by the calibration process (which assumes a constant non-linearity correction). However, the nonlinearities measured before launch were relatively small and cannot account for the large bias changes in channels 13 and 14. Furthermore, if this were the cause we would expect to see geographical changes occurring with these jumps, since errors in the non-linearity correction affect observations differently depending on the scene temperature (Lu et al.,

Table 5: Pearson's Correlation Coefficient for correlations between observation minus ECMWF background statistics for MWHS-2 channels and the mean environment instrument temperature of MWHS-2. Also given are the slopes of the linear best fit, for both ECMWF and Met Office O - B values. Also given are approximate magnitude of the O - B bias change from March to May 2016, for channels where an obvious change occurred.

MWHS-2 Channel Number	Correlation Coefficient		Best fit slope (K/K)		Magnitude of bias change	
	ECMWF	Met Office	ECMWF	Met Office	ECMWF	Met Office
1	-0.02	0.30	0.00	0.09	-	-
2	0.50	0.67	0.06	0.07	0.5	0.5
3	0.78	0.88	0.06	0.07	0.3	0.3
4	0.85	0.91	0.07	0.07	0.3	0.4
5	0.39	0.44	0.01	0.01	0.6	0.7
6	0.82	0.80	0.04	0.03	0.14	0.2
7	-0.33	-0.26	-0.01	-0.01	-	-
8	-0.43	-0.12	-0.02	-0.01	-	-
9	- 0.59	-0.23	-0.08	-0.03	-	-
10	- 0.31	0.06	-0.05	0.01	-	-
11	0.73	0.73	0.06	0.05	0.75	0.2
12	0.66	0.62	0.04	0.04	0.2	0.8
13	-0.94	-0.95	-0.30	-0.34	-1.2	-1.7
14	-0.95	-0.95	-0.52	-0.57	-2.2	-2.5
15	-0.57	-0.32	-0.03	-0.02	-	-

2011).

While we do not yet understand the causes of these bias changes, it is worth noting that these jumps in bias are small for most channels and are successfully removed by the Variational Bias Correction schemes at ECMWF and the Met Office so that the data can still be assimilated. Indeed the assimilation of MWHS-2 data was found to have a positive impact on forecast accuracy, despite these jumps in bias (Lawrence et al., 2017). For channels 13 and 14 however the bias changes are relatively large and these channels are not assimilated at ECMWF, pending further investigation of the causes.

9 O - B statistics for MWRI

9.1 Ascending-Descending biases for MWRI

Maps of O - B over a 12-hour period show a clear bias difference between the ascending and descending orbits of MWRI for all channels. This can be seen for both ECMWF statistics and the Met Office statistics, and is illustrated in Fig. 5 for the 10H and 23V channels. The magnitude of this ascending-descending bias is approximately 2 K for all channels for both ECMWF and Met Office statistics, as shown in Fig. 6.

An ascending-descending bias is not observed for the equivalent channels of AMSR-2 (not shown), which gives us some confidence that this bias is instrument-related. Ascending-descending biases have been observed previously for other imagers including F-16 SSMI/S, however (Bell et al., 2008). For this instrument the ascending-descending bias was diagnosed to be due to solar heating of the reflector leading to an emission which varied depending on whether the instrument was in the sunlight or the shade. Similar solar-dependent biases were seen also for the TMI instrument (Geer et al., 2010) and

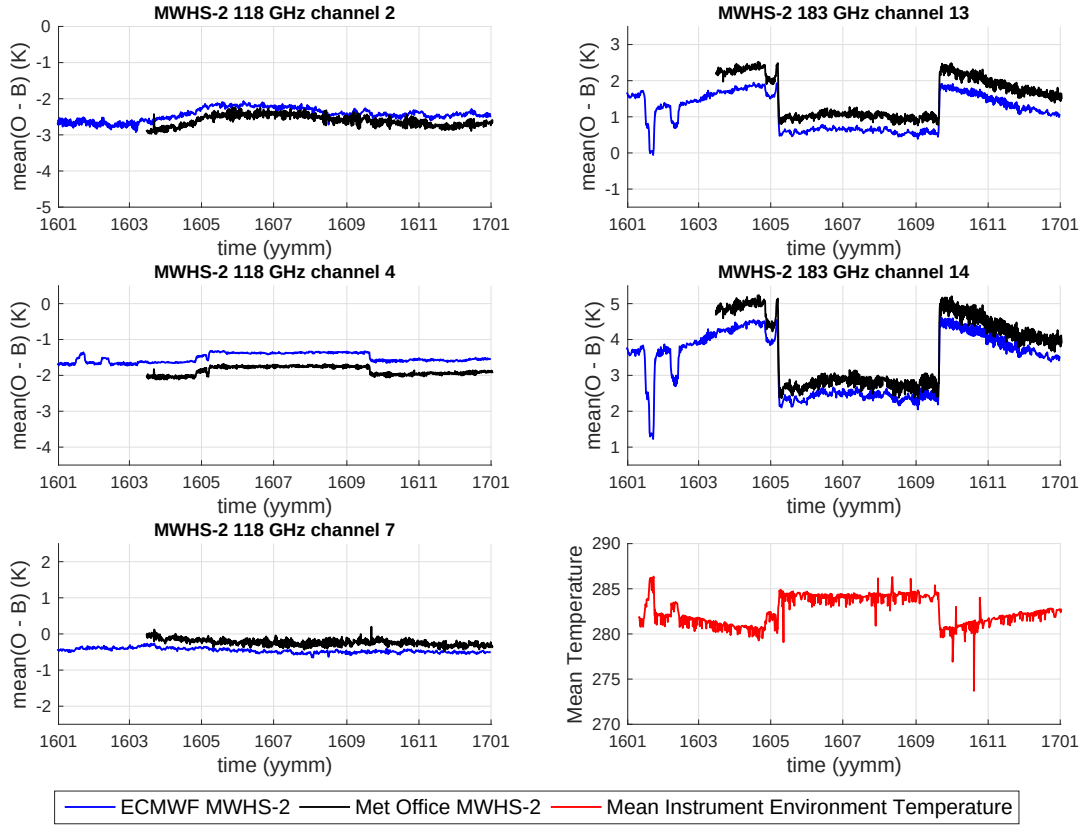

Figure 3: Changes in the mean O - B for MWHS-2 channels, plotted as a function of time for channels 2, 4, 7, 13 and 14. The change in environent instrument temperature is also shown. Environment instrument temperature values are taken from the Met Office direct broadcast data.

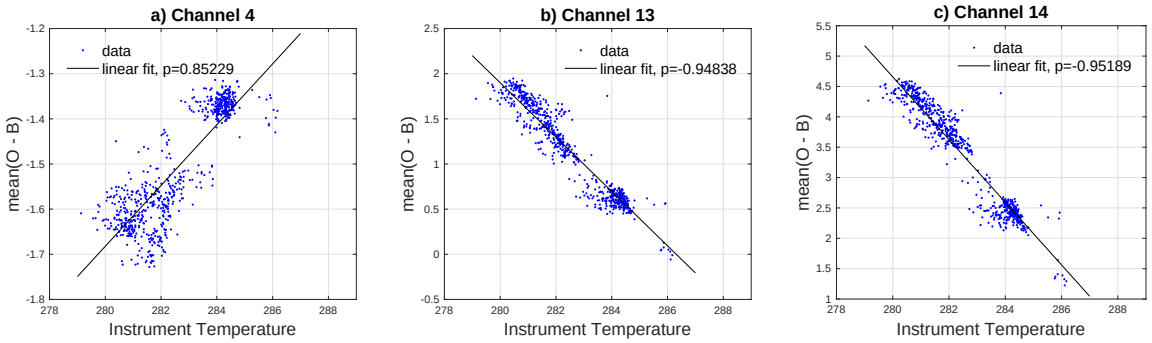

Figure 4: MWHS-2 mean observation minus ECMWF background plotted as a function of environment instrument temperature for 3 channels: channels 4, 13 and 14. A Linear regression is also plotted for each channel's data, and Pearson's correlation coefficient is given in the legend.

these biases were found to be geographically complex and to vary with the season. Potential emission of the main reflector could not be the cause of ascending-descending biases for MWRI since the calibration process removes the effects of the reflector. However, it is possible that there is emission from other parts of the instrument which are not removed by the calibration process, for example the warm load reflector. It is also possible that there is contamination into the warm load view from the Earth scene, which has not been completely removed by the calibration process.

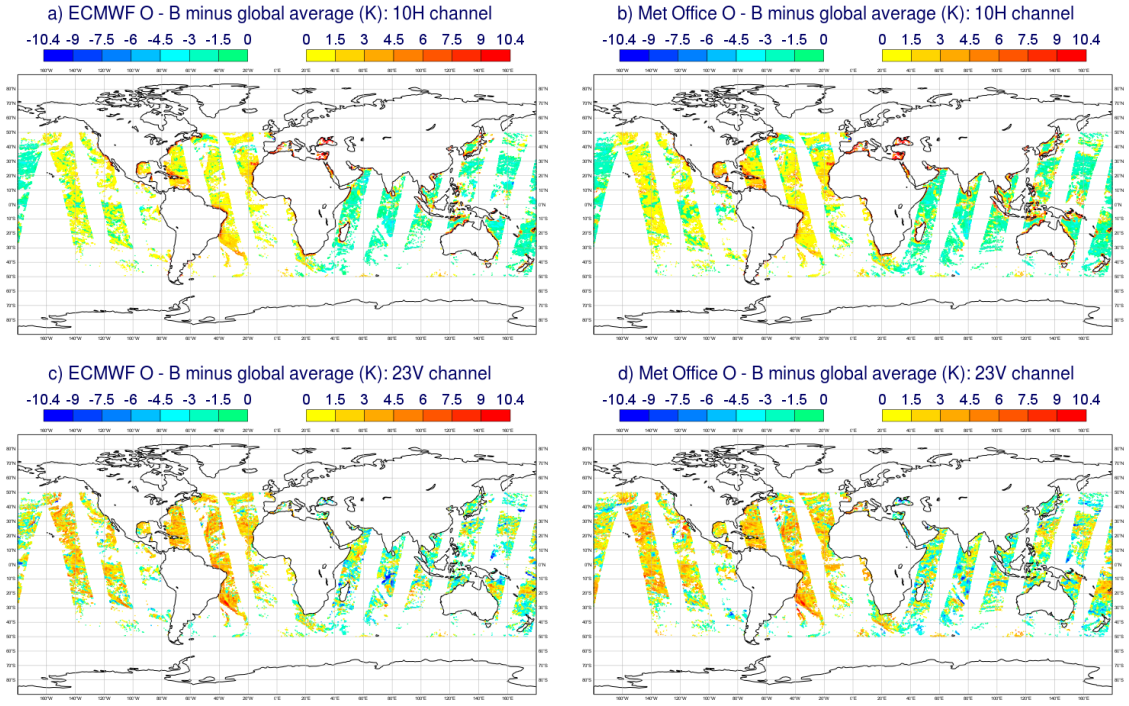

Figure 5: O - B for MWRI for a 12-hour period on 15 September 2016, shown for a) 10H channel, ECMWF statistics, b) 10H channel, Met Office statistics, c) 23V channel, ECMWF statistics, and d) 23V channel, Met Office statistics.

Maps of mean observation minus background averaged over 1 month also show differences for ascending and descending data, indicating that the ascending-descending bias has a geographical structure within the half orbits. This is shown in Fig. 7 for the 37V MWRI channel, plotted for both the ECMWF and Met Office data. Note that the maps for the Met Office and ECMWF data appear to be quite different for this channel. Possible causes for this include different biases in the humidity background value at ECMWF and the Met Office, or residual cloud which is treated differently in the all-sky and clear-sky systems. Further work is needed to understand this. Despite this difference, there is a consistent pattern between ECMWF and Met Office data showing that the ascending data are warmer than descending data in the Northern Hemisphere and cooler than descending data in the Southern Hemisphere. This is a pattern which is not observed for AMSR-2, also plotted in Fig. 7. (Note that the gaps in data for AMSR-2 here are due to a longitude screen being used together with a time screen to separate ascending and descending data.) This is consistent with what we would expect of biases that have a structure around the orbit of the instrument, such as solar-dependent biases or contamination from the Earth into the warm load view.

A 2 K ascending-descending bias for MWRI is larger than previously seen for similar instruments, and such a bias should be corrected before the data could be assimilated in NWP or reanalysis systems. One solution is to develop an empirical correction, such as a correction based on the orbital angle (Booton et al., 2014) or the solar hour (Geer et al., 2010). However, if the causes of the bias could be better

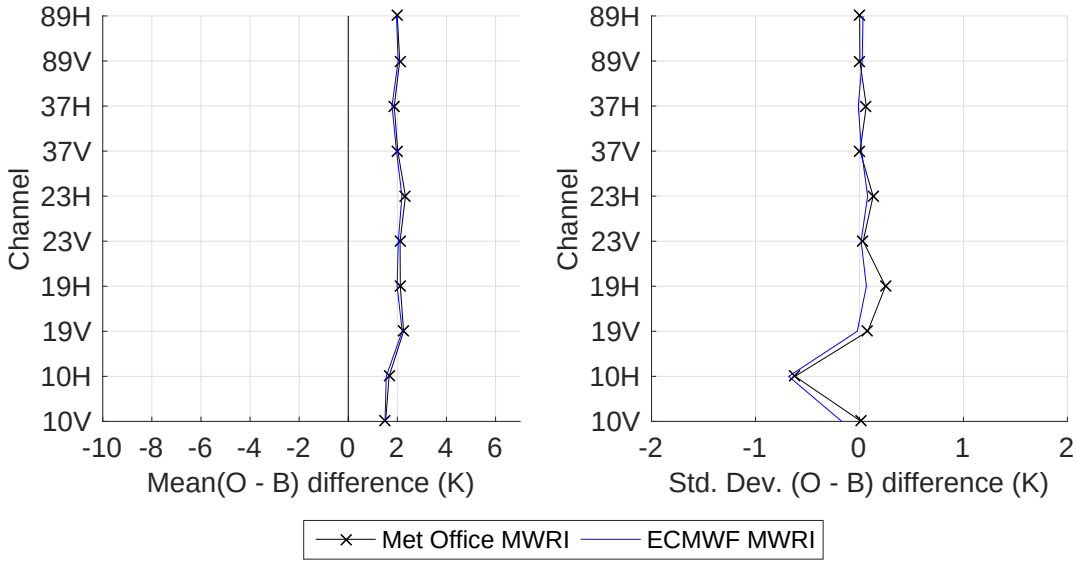

Figure 6: Mean and Standard Deviation of O - B for MWRI ascending data minus equivalent values for descending data, for both ECMWF and Met Office statistics. Statistics are calculated for ocean data only, with a latitude less than 50 degrees, and after applying a cloud screening.

understood this could guide the development of future instruments and could potentially also lead to a more physical correction for FY-3C MWRI.

9.2 Radio Frequency Interference at 10.65 GHz

Maps of mean O - B averaged over 1 month for the 10V/H channels of MWRI clearly show large positive values in a localised area around Europe, for both ECMWF and Met Office statistics. This can be seen in Fig. 8. Maps of O - B for individual satellite passes show further that these warm biases are visible for the descending passes only, as shown in Fig. 9. The pattern of these biases suggests that they are due to Radio Frequency Interference (RFI) from a geostationary satellite. A possible candidate for this would be the Astra communication satellites, operated by Société Européenne des Satellites (SES), which are the major television satellites serving Europe, North Africa, Western Russia and the Middle East. They operate in the 10.7 GHz - 12.7 GHz bands and are located at 5°E, 19.2°E, 23.5°E, 28.2°E and 31.5°E[3]. Fig. 10 illustrates the geometry of potential interference from an emitting geostationary satellite. The MWRI instrument is forward-looking so that, as the FY-3C satellite descends over the North pole and towards Europe, the instrument is at the right viewing angle to capture the emission of a satellite situated at the equator, reflected off the surface of the ocean. The instrument scans in a circular motion across the swath, at a constant zenith angle of 53°, which leads to reflection conditions being met only for certain scan positions. This is why the interference occurs for only part of the swath. Furthermore, for each swath the geostationary satellite is in a different position relative to the descending polar-orbiting satellite, so that the reflection conditions are met for different scan positions in each swath. This is consistent with the pattern seen in Fig. 9. Note that RFI was also observed around the West coast of North America for the 19 GHz channels. This is known RFI that was identified previously for AMSR-E and AMSR-2 instruments (Kazumori et al., 2016, Newman et al., 2016, International TOVS working group).

[3]Details of these satellites can be found on the ses website at https://www.ses.com

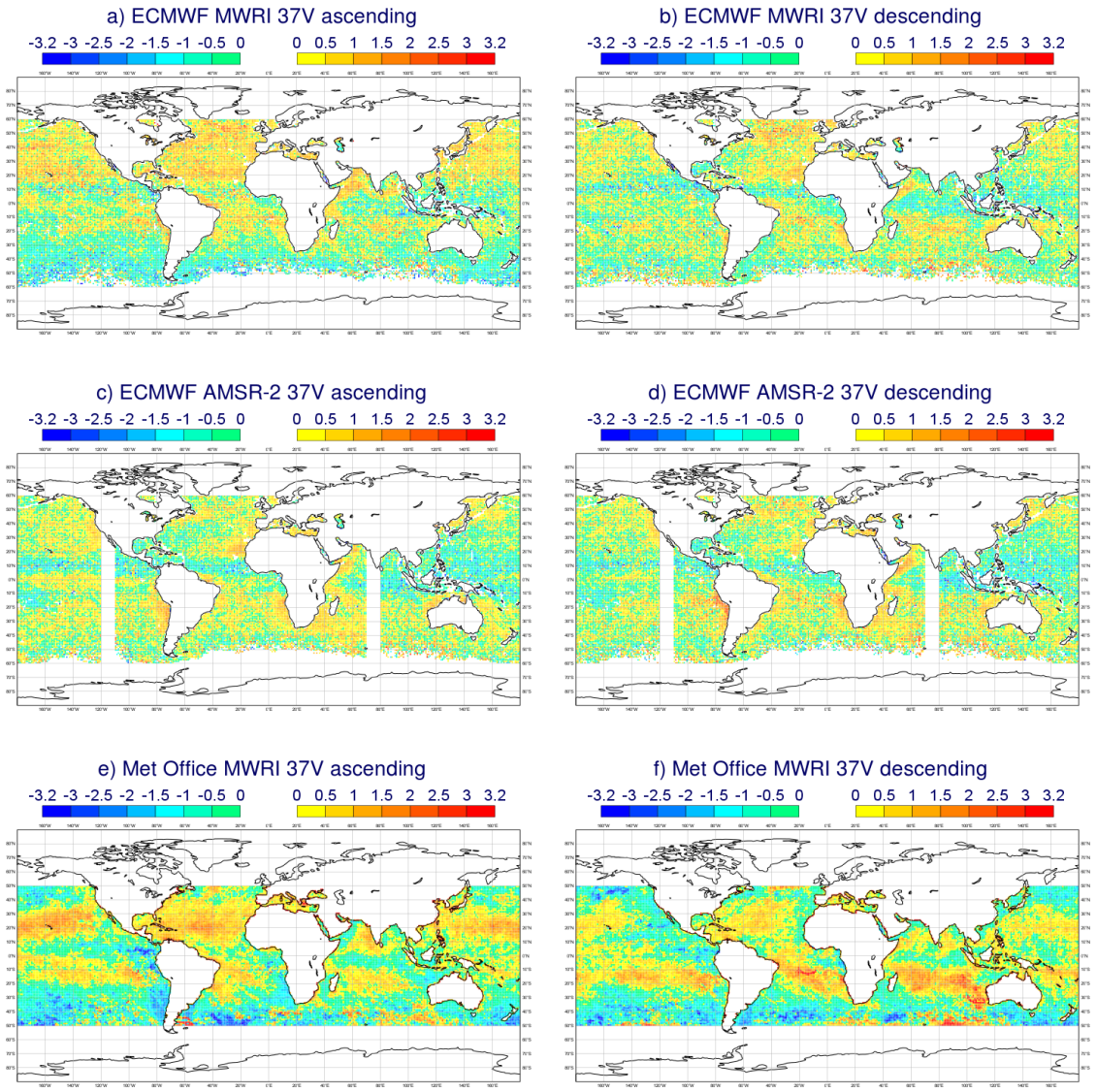

Figure 7: Mean O - B averaged over 1 month (September 2016) shown for a) ECMWF background fields, MWRI 37V channel ascending only data, b) ECMWF background fields, MWRI 37V channel descending only data, c) ECMWF background fields, AMSR-2 37V channel ascending only data, d) ECMWF background fields, AMSR-2 37V channel descending only data, e) Met Office background fields, MWRI 37V channel ascending only data, and f) Met Office background fields, MWRI 37V channel descending only data.

The RFI for the 10V/H channels can also be seen in maps of observation minus background for the AMSR-2 instrument (descending data), as shown in Fig. 11. The RFI appears to be less strong for AMSR-2, however, and it would have been difficult to identify without looking first at statistics for MWRI. The weaker RFI for AMSR-2 can be explained by different bandwidths for the 10.65 GHz channels of these two instruments. MWRI has a specified bandwidth of 180 MHz whereas AMSR-2 has a narrower specified bandwidth of 100 MHz leading to an upper frequency limit of 10.74 GHz for MWRI and 10.70 GHz for AMSR-2. This is enough for MWRI to suffer interference from communications satellites emitting at 10.7 - 12.7 GHz. We would also expect to see some interference for the AMSR-2 observations, since the 100 MHz bandwidth refers to the 3 dB bandwidth and there are likely to also be small contributions at frequencies above 10.7 GHz. This depends on the shape of the spectral response function for the 10.65 GHz channels of AMSR-2, however.

Communications satellites operating in the range of 10.7 - 12.7 GHz are not illegal since this frequency band is not protected. The frequency range 10.68 - 10.70 GHz is protected, however, and so it would be worth checking that there is no emission from the geostationary satellites below 10.70 GHz. To do this, it would be useful to have the measured spectral response functions for the 10 GHz channels and so it would be worth the satellite agencies making these available. In addition, satellite agencies should consider taking steps in the future to keep the bandwiths of the 10.65 GHz channels within the protected band. This would prevent further interference from communications satellites operating at 10.7 GHz.

The 10.65 GHz channels onboard microwave imagers are currently not operationally assimilated at either ECMWF or the Met Office but it could be desirable to assimilate these channels in the future, since they could provide useful information in NWP and reanalysis systems, particularly in areas of heavy precipitation over ocean. Before attempting to assimilate these channels a successful RFI filtering method over Europe would need to be developed. One option for this would be to filter using the glint angles from the relevant geostationary communications satellites.

9.3 Global O - B statistics

Histograms of all O - B values for MWRI are very similar for both NWP centres. This is shown in Fig. 12 for the ascending data of MWRI. The biases and standard deviation of O - B are also similar between the two NWP centres for most channels, as shown in Fig. 13. This is in contrast to the large bias differences observed previously for AMSR-2 (Newman et al. (2016)) and is further proof that these biases were due to a different FASTEM model being used. The statistics for both ECMWF and Met Office data indicate that MWRI has negative biases relative to NWP background fields for most channels (note that the biases for descending data are 2 K lower). AMSR-2 on the other hand has positive biases relative to the ECMWF background, as shown in Fig. 13, and so there is a bias difference between AMSR-2 and MWRI of at least 3 K (3 - 5 K for MWRI ascending data and 5 - 7 K for descending data).

The results presented here illustrate the value of using NWP short-range forecasts in the cal/val of new satellite instruments. Despite differences between the ECMWF and Met Office systems, the results show consistent biases for MWRI. In addition, the use of a forecast model allows us to compare the data for AMSR-2 and MWRI, while accounting for geophysical differences in the observations due to differences in the satellite overpass times (13:30 ascending for GCOM-W1 AMSR-2 and 10:15 descending for FY-3C MWRI). It is difficult to put error bars on the estimates of either the absolute bias or the intersatellite bias between MWRI and AMSR-2, however. To do this we would need to know the uncertainties in the NWP background fields, uncertainties in the radiative transfer models and emissivity models used, uncertainties in spatial mismatch errors (representivity errors) and uncertainties in the cloud screening approach. During the GAIA-CLIM project we aim to address some of these uncertainties, so that we

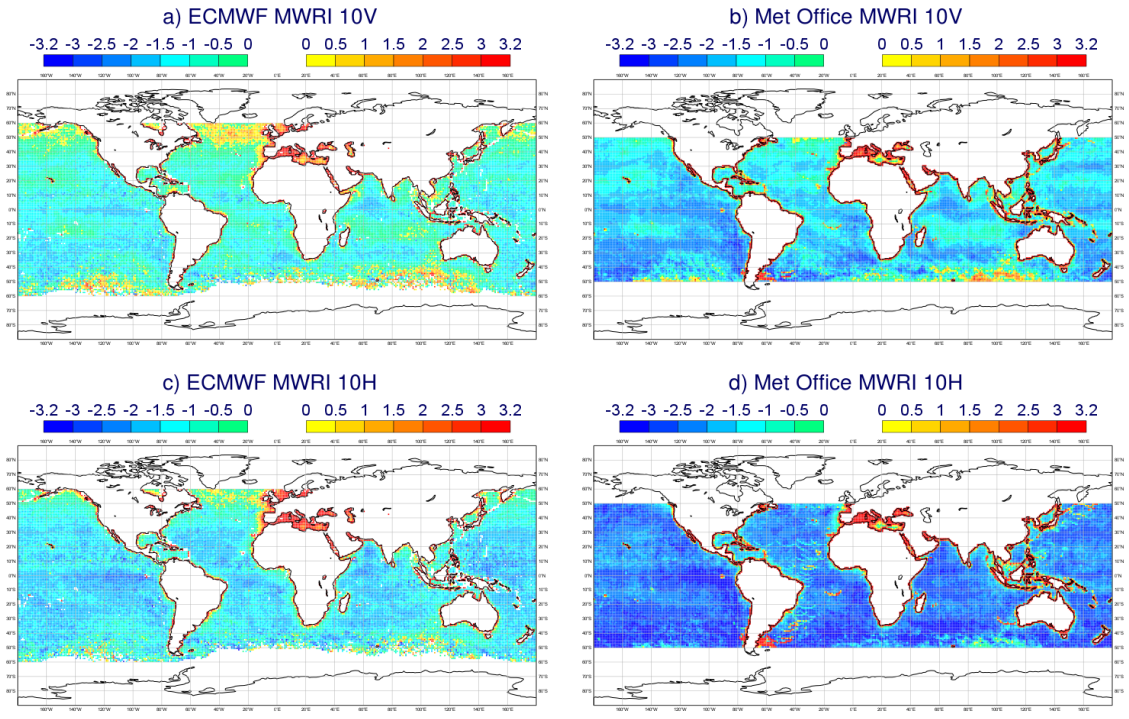

Figure 8: Mean O - B averaged over 1 month (September 2016) for a) ECMWF background fields, MWRI 10V channel, b) Met Office background values, MWRI 10V channel, c) ECMWF background fields, MWRI 10H channel, and d) Met Office background values, MWRI 10H channel.

can start to put error bars on the biases found using NWP. Remaining sources of uncertainty will also be identified and outlined in the Gap Analysis and Impacts Document (GAID) provided by the GAIA-CLIM project.

It will also be interesting to revisit these biases after the evaluation of the the Global Precipitation Measurement (GPM) Microwave Imager (GMI), planned for the 3rd year of the GAIA-CLIM project. GMI is thought to be a very well-calibrated imager with calibration uncertainties of 0.25 K over ocean (Draper et al., 2015, Wentz and Draper, 2016). GMI is currently assimilated at ECMWF and O - B statistics show low biases ($\sim$0.9K in magnitude) for the equivalent channels to MWRI (Lean et al., 2017), which firstly is a good indication of low biases in the NWP background fields and secondly could provide us with an additional estimate of the uncertainties associated with using NWP as a reference for the validation of imagers. This will be explored further in year 3 of the GAIA-CLIM project with a joint evaluation of GMI statistics at ECMWF and the Met Office.

The standard deviation of O - B for MWRI (shown in Fig. 13) is similar for ECMWF statistics and Met Office statistics for most channels. The standard deviation is higher for the Met Office statistics, however, for the 10V/H channels. This is most likely just the effect of some spurious data for these channels which have been included in the Met Office statistics, as indicated by some bad scanlines visible in the monthly maps shown in Fig. 8. There is an initial check carried out on the data in the ECMWF system which would remove these bad scanlines before the data are processed and hence they are not included in the ECMWF statistics for these channels (see Fig. 8).

The standard deviation of O - B is also larger for MWRI than for AMSR-2 for some channels. The larger standard deviations for the lower frequency channels can be explained by a larger field of view leading to

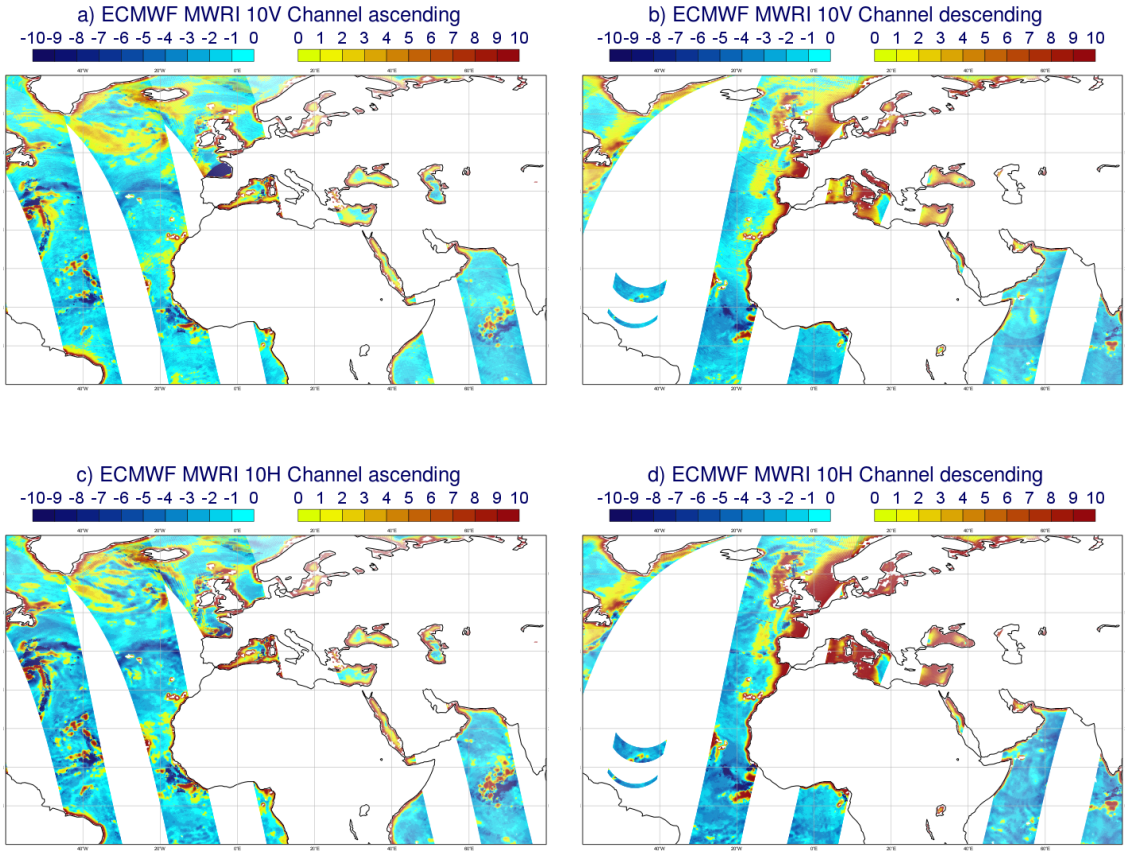

Figure 9: O - B values minus the global average for the 10V/H channel of MWRI on 2016091500 and 2016091512, shown for ECMWF background fields only, for a) the 10V channel, ascending only data, b) the 10V channel, descending only data, c) the 10H channel, ascending only data, and d) the 10H channel, descending only data.

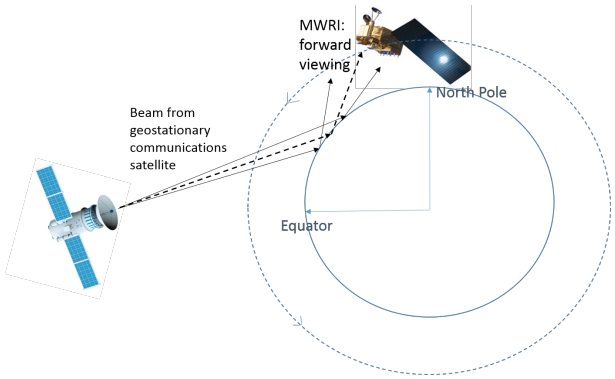

Figure 10: Geometry of radiofrequency interference from a geostationary communications satellite.

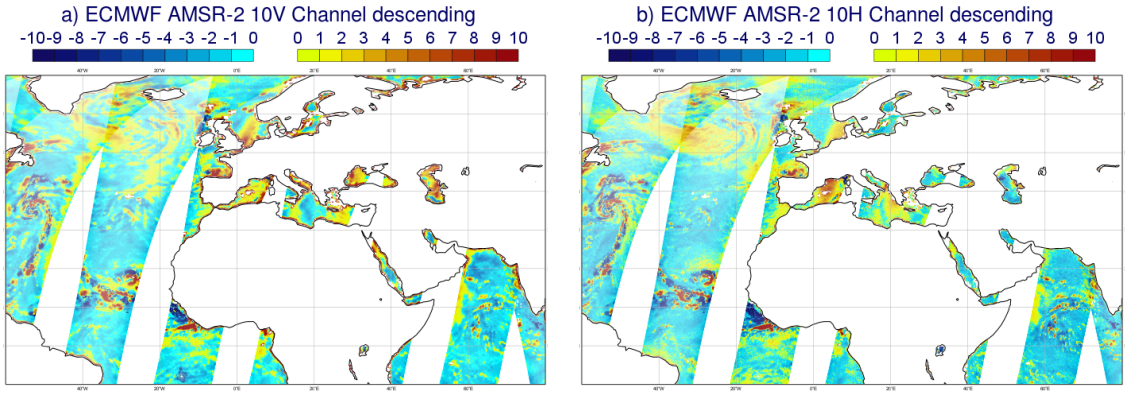

Figure 11: O - B values minus the global average for descending only data for AMSR-2 on 2016091500 and 2016091512, sshown for ECMWF background fields only, for a) 10V channel and b) 10H channel.

some land contamination around the coastlines for the MWRI channels. This can be seen in Fig. 9 with a smaller effect seen for AMSR-2 in Fig. 11. For these channels the land screening has not removed all of the land-contaminated data since the field of view size is larger than the resolution of the land-sea mask used in the NWP systems. The higher standard deviation of O - B for the 23V/H channels, however, can not be explained by land contamination and this requires some further investigation. Possible causes include the ascending-descending bias, which has been found to also have a structure within the half-orbits, or larger spatial mismatch errors (representivity errors) for MWRI.

9.4 Time series of O - B statistics for MWRI

The observation minus background values were monitored for MWRI at ECMWF and the Met Office from August 2016 to the present. The time series of O - B for all channels show slow drifts in global biases during this period, which occurs at a similar rate for both NWP centres. This can be seen in Fig. 14 which shows the mean O - B minus the time averaged value, as a function of time for all channels and both NWP centres. Note that the lower variability for ECMWF statistics compared to Met Office statistics is due to the superobbing, which is applied to the observations for ECMWF statistics in this plot. The drifts in bias were observed for ascending and descending data, as well as all data, as illustrated in Fig. 15 which shows the change in bias for the 19V channel of MWRI (ECMWF statistics only). Mean O - B is also plotted for ECMWF for the period of June - August 2014, using a small sample dataset provided by CMA. This shows that the difference in the biases of ascending and descending data has increased from 1 K to 2 K over the last 2 years.

These statistics indicate that the biases of MWRI are not stable over time. The observed drifts may be another indication of the ascending-descending bias, however, or this may be a separate effect. This depends on the mechanism causing the ascending-descending biases and further investigation of the sources of this bias may confirm this. For example, it would be useful to monitor the MWRI biases over a full year, as this should show if the drifts are seasonal or not.

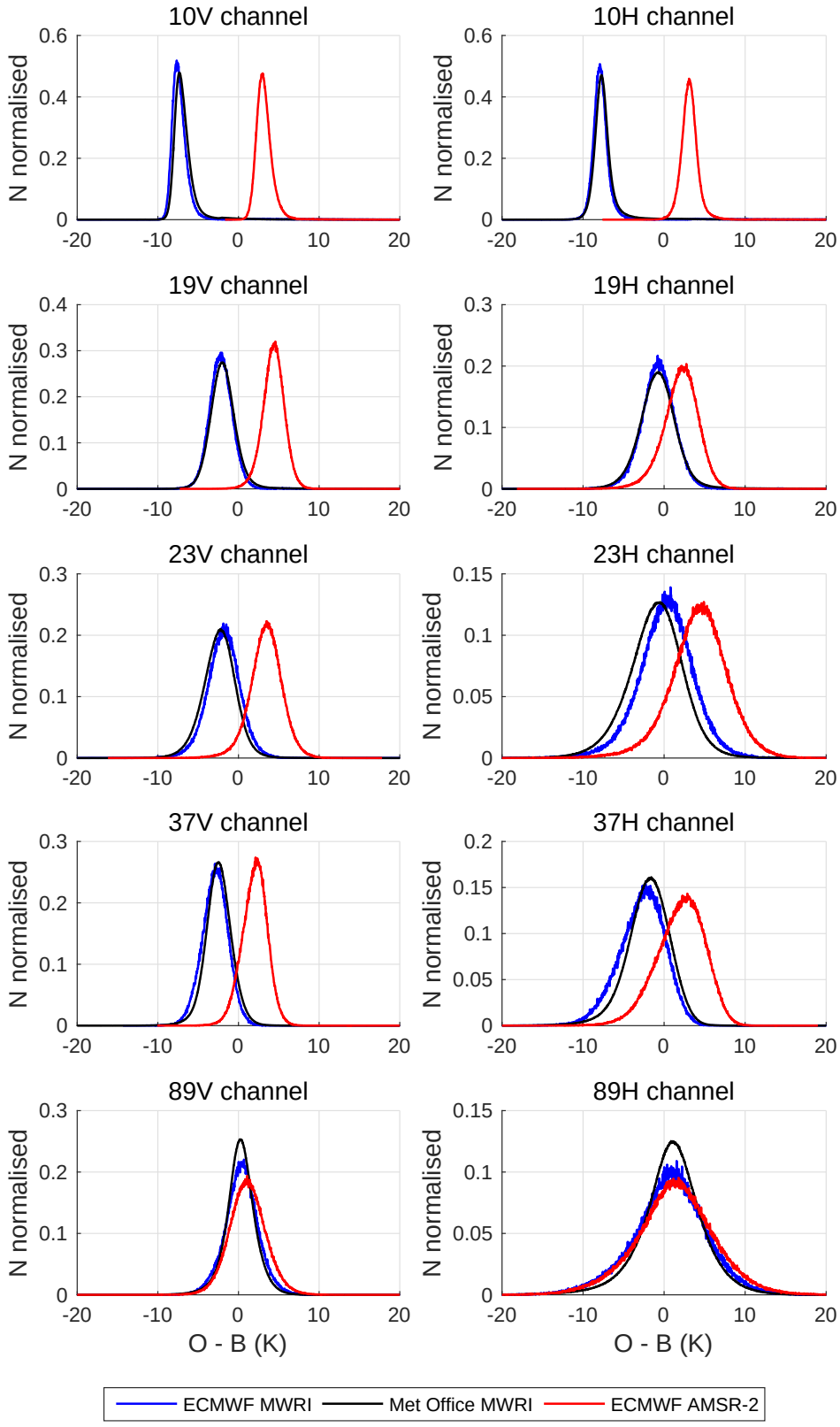

Figure 12: Histograms of the O - B values for the ascending data of MWRI (both ECMWF and Met Office statistics) and AMSR-2 (ECMWF statistics, ascending and descending combined), after cloud screening and over ocean only with a latitude less than 50 degrees.

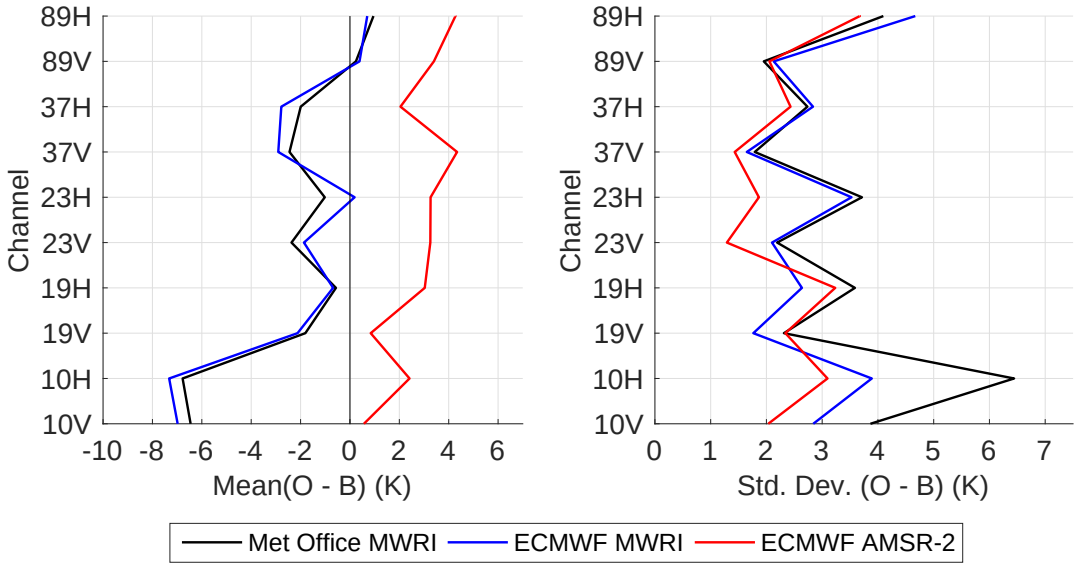

Figure 13: Mean and Standard Deviation of O - B for MWRI ascending data (Met Office and ECMWF) and AMSR-2 all data (ECMWF). Statistics are calculated for ocean data only, with a latitude less than 50 degrees, and after applying a cloud screening.

10 Conclusions

In this study, we have assessed the long-term performance of the FY-3C MWHS-2 instrument and performed a first assessment of the quality of the FY-3C MWRI microwave imager instrument, using observation minus background statistics from the ECMWF and Met Office NWP systems. The main results were as follows.

For MWHS-2:

- The assessment of MWHS-2 showed a number of jumps in mean O - B over 2016 for most channels which were observed consistently for ECMWF and the Met Office statistics. These were found to be correlated to changes in the environment temperature of the instrument. These jumps in bias were of the order 0.2 - 0.3 K for most channels with the exception of channels 13 and 14 which showed jumps of magnitude 2 - 3 K.

For MWRI:

- Different biases were observed for the ascending and descending passes of the instrument of approximately 2 K in magnitude for both ECMWF and Met Office statistics. Maps of observation minus background averaged over 1 month also indicated different geographical patterns for ascending and descending data for both the Met Office and ECMWF. This is reminiscent of the complex solar-dependent biases observed previously for the early SSMI/S instruments. The magnitude of the bias is larger than observed previously for other imagers, however.
- RFI was found around Europe for the 10.65 GHz channels of MWRI (descending only data), with patterns consistent with interference from a geostationary communications satellite. The RFI is also visible for the AMSR-2 instrument but is weaker due to a narrower bandwidth.

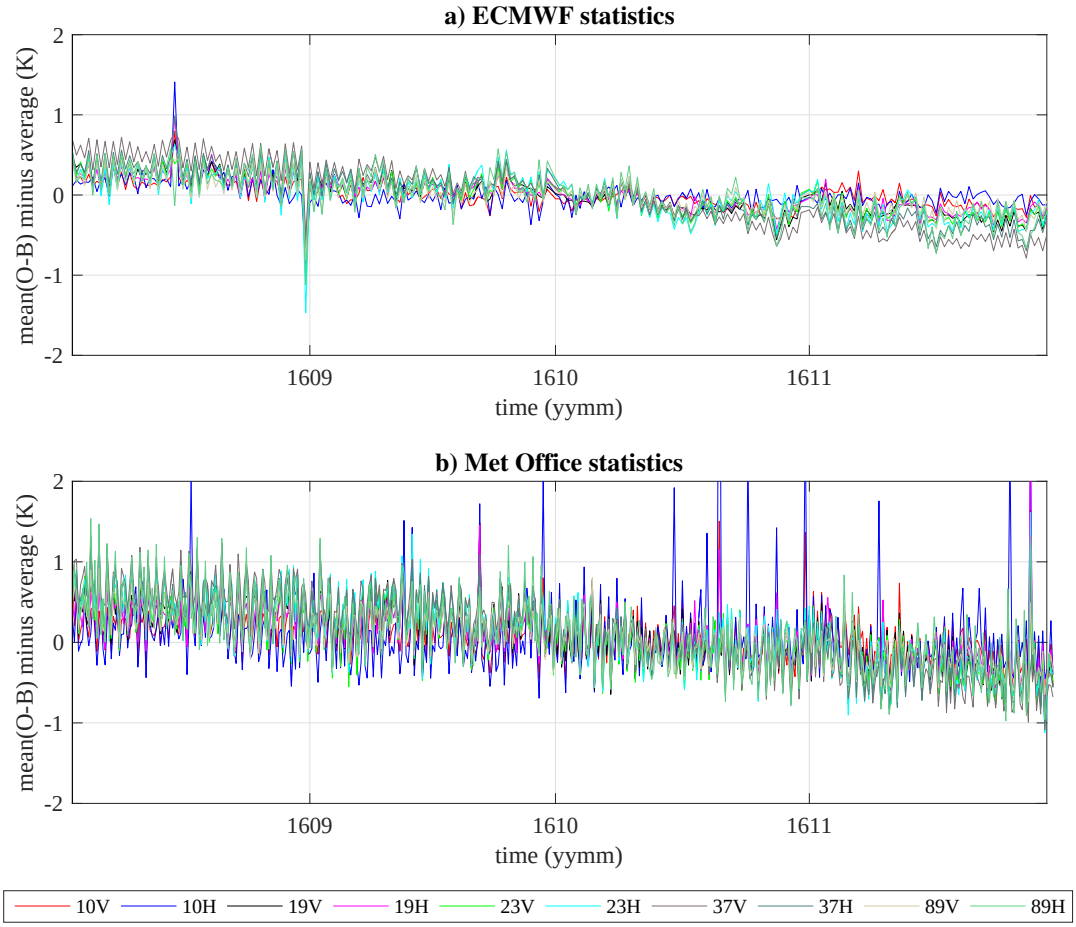

Figure 14: Timeseries of O - B for all MWRI channels, minus the time-averaged value and shown for a) ECMWF background fields and b) Met Office background fields. Note that the observations were superobbed before calculating the observation minus background values in the ECMWF system and the background fields for the Met Office data were calculated using older version of FASTEM-2 and RTTOV-9.

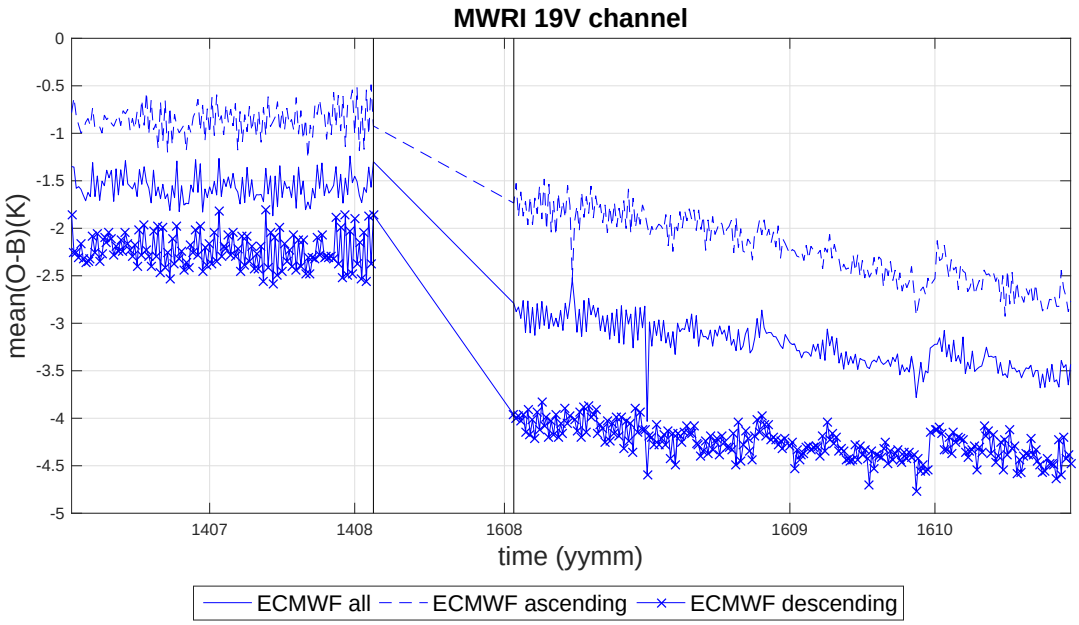

Figure 15: Timeseries of O - B for the 19V channels of MWRI for ECMWF background fields, over ocean only and after the cloud and latitude screening. Note that the observations were superobbed before calculating the observation minus background values.

- MWRI channels have negative biases in comparison to the short-range forecasts of ECMWF and the Met Office, compared to positive biases for AMSR-2. This indicates an intersatellite bias between AMSR-2 and MWRI of around 4 - 6 K, depending on the channel.
- Time series showed bias drifts for all channels of MWRI over the period August - December 2016, consistent for both the Met Office and ECMWF data. In addition the ascending-descending bias has increased in magnitude from 1 K to 2 K over the last 4 years.

The changes in bias for MWHS-2 over the last year do not preclude the use of the data in NWP and reanalysis systems, since for most channels the magnitude of the change is small and in addition it appears to be a global effect. These bias changes can therefore be corrected by the adaptive bias correction schemes employed at both centres, and the assimilation of this data has been shown to improve forecast accuracy (Lawrence et al., 2017). Channels 13 and 14 suffered relatively large bias changes of respectively 2 K and 3 K, however, and these channels now have a much higher magnitude of bias than equivalent channels of other instruments. It would therefore be desirable to further understand the causes of these biases, and if possible correct them in the level 1 data.

The biases observed for MWRI, however, make it difficult to assimilate these data into NWP and/or reanalysis systems, unless a successful bias correction scheme can be developed. The ascending-descending bias in particular is larger than observed for previous instruments and also has a geographical structure which must be corrected. It may be possible to successfully correct such biases, however, for example using the oribital angle as a bias predictor as done by Booton et al. (2014) for the SSMI/S instrument. It would also be useful to further investigate the causes of the bias, since this could lead to better data for future MWRI instruments and possibly a more physical correction for FY-3C MWRI.

It is worth noting that MWRI is of potential value in regional as well as global NWP, because it is the only current microwave imager whose data are readily available by direct broadcast. So timeliness of order

15 minutes is achievable, allowing the data to be ingested within the short cutoff times of operational regional models. Successful implementation in regional NWP will be dependent on the bias problems being solved using global NWP, however.

The assessment of MWRI and MWHS-2 presented in this report demonstrates the usefulness of NWP short-range forecasts for assessing new satellite instruments. In particular a comparison between statistics for the Met Office and ECMWF has allowed us to identify biases that are consistent with both NWP centres as being likely due to the instrument. Using NWP forecasts as a reference has also allowed us to make comparisons to similar instruments such as AMSR-2, since the forecast model removes differences due to different observation times. For example the results presented here have indicated a large intersatellite bias of around 4 - 6 K between AMSR-2 and MWRI.

Despite being able to identify different types of bias and estimate intersatellite biases in this assessment, it is difficult to place uncertainties on the values obtained. To do this we would need to know the uncertainties in the NWP background fields, the radiative transfer and surface emissivity models, and uncertainties due to the scale mismatches between the observations and model, and to the cloud detection scheme. Work is ongoing to assess the NWP background temperature and humidity fields using the GRUAN network as a reference. The lack of uncertainties in radiative transfer calculations, surface emissivity models and scale mismatches have been identified as gaps for the calibration/validation of imagers and sounders and suggestions for the resolution of these gaps have been made in the Gap Analysis and Impacts Document (GAID) provided by the GAIA-CLIM project. We aim to resolve in some part these issues during the GAIA-CLIM project.

An additional uncertainty contribution (to the simulated radiances) arises from the impact of undetected cloud. For the purposes of validating measured satellite radiances it is sensible to select measured scenes that are free of the radiative impact of cloud. This is accomplished using some form of cloud screening, based on the measured and simulated radiances. The process is generally imperfect though and there are normally residual cloud impacts on scenes identified as nominally clear. This can be a significant issue for microwave imagers which sense the entire atmospheric column and are therefore sensitive to clouds at lower levels. One way to estimate uncertainties due to imperfect cloud detection would be to apply the method used by Sreerekha et al. (2010). This method uses the difference in background fields calculated in clear-sky and all-sky conditions, using RTTOV and RTTOV-SCATT, as simulated O - B values. The cloud-screening is then applied and the standard deviation of simulated O - B after screening gives an estimate of the uncertainties.

Acknowledgements

The work presented in this report was funded by the the European Union's Horizon 2020 research and innovation programme under the GAIA-CLIM project (grant agreement No. 640276). This work has benefitted from an ongoing collaboration with the China Meteorological Administration (CMA) National Satellite Meteorological Centre (NSMC), and in particular Dr. Qifeng Lu, and we gratefully acknowledge NSMC for their help in understanding the instrument characteristics, and discussions of possible sources of bias in the O - B statistics.

References

P. Bauer, E. Moreau, F. Chevallier, and U. O'Keeffe. Multiple-scattering microwave radiative transfer for data assimilation applications. *Quart. J. Roy. Meteorol. Soc.*, 132:1259 – 1281, 2006.

W. Bell, B. Candy, N. Atkinson, F. Hilton, N. Baker, N. Bormann, G. Kelly, M. Kazumori, W.F. Campbell, and S.D. Swadley. The assimilation of SSMIS radiances in numerical weather prediction models. *IEEE Trans. Geoscience. Rem. Sensing.*, 46:884 – 900, 2008.

A. Booton, W. Bell, and N. Atkinson. An improved bias correction for SSMIS. *Proceedings of the International TOVS Study Conference (ITSC) 19, Jeju Island, South Korea*, 2014.

D. W. Draper, D. A. Newell, F. J. Wentz, S. Krimchansky, and G. M. Skofronick-Jackson. The global precipitation measurement (GPM) microwave imager (GMI): Instrument overview and early on-orbit performance. *IEEE Journal of Selected Topics in Applied Earth Observations and Remote Sensing*, 8: 3452–3462, 2015.

A.J. Geer and P. Bauer. Enhaced use of all-sky microwave observations sensitive to water vapour, cloud and precipitation. *ECMWF Tech. Memo.*, 620, 2010.

A.J. Geer, P. Bauer, and N. Bormann. Solar biases in microwave imager observations assimilated at ECMWF. *IEEE Trans. Geoscience. Rem. Sensing.*, 48:2660–2669, 2010.

International TOVS working group. Radio Frequency Interference (RFI) and NWP. URL https://groups.ssec.wisc.edu/groups/itwg/nwp/rfi_and_nwp/.

H. Jieying, Z. Shengwei, and W. Zhenzhan. Advanced microwave atmospheric sounder (AMAS) channel specifications and T/V calibration results on FY-3C satellite. *IEEE Trans. Geoscience. Rem. Sensing.*, 53:481 – 493, 2015.

M. Kazumori, A. J. Geer, and S. J. English. Effects of all-sky assimilation of GCOM-W/AMSR2 radiances in the ECMWF numerical weather prediction system. *Quart. J. Roy. Meteorol. Soc.*, 142:721 – 737, 2016.

H. Lawrence, N. Bormann, A. Geer, Q. Lu, and S.J. English. Evaluation and assimilation of FY-3C MWHS-2 at ECMWF. *IEEE Trans. Geosci. Remote Sens.*, submitted, 2017.

P. Lean, A. Geer, and K. Lonitz. Assimilation of Global Precipitation Mission (GPM) Microwave Imager (GMI) in all-sky conditions. *ECMWF Tech. Memo.*, in preparation, 2017.

K. Lonitz and A. Geer. New screening of cold-air outbreak regions used in 4D-Var all-sky assimilation. *EUMETSAT/ECMWF Fellowship Programme Research Report*, 35, 2015.

Q. Lu, W. Bell, P. Bauer, N. Bormann, and C. Peubey. Characterizing the FY-3A microwave temperature sounder using the ECMWF model. *J. Atmos. Oceanice Technol.*, 28:1373–1389, 2011.

Q. Lu, H. Lawrence, N. Bormann, S. English, K. Lean, N. Atkinson, W. Bell, and F. Carminati. An evaluation of FY-3C satellite data quality at ECMWF and the Met Office. *ECMWF Tech. Memo.*, 767, 2015.

S. Newman, W. Bell, and K. Salonen. Calibration/validation study of AMSR-2 on GCOM-W1. *GAIA-CLIM Deliverable 4.2, available online*, 2016. URL http://www.gaia-clim.eu.

R. Saunders, M. Matricardi, and P. Brunel. An improved fast radiative transfer model for assimilation of satellite radiance observations. *Q. J. R. Meteorol. Soc.*, 125:1407–1425, 1999.

T. R. Sreerekha, A. Doherty, and S. English. Potential of 229-Ghz channel for ice-cloud screening. *IEEE Trans. Geoscience. Rem. Sensing.*, 48:2183–2188, 2010.

F. J. Wentz and D. Draper. On-orbit absolute calibration of the global precipitation measurement microwave imager. *Journal of Atmospheric and Oceanic Technology*, 33:1393–1412, 2016.

H. Yang, L. Lv, N. Lu, G. Liu, M. Bai, Q. Qian, J. He, and H. Xu. The Feng-Yun-3 microwave radiation imager on-orbit verification. *IEEE Trans. Geoscience. Rem. Sensing.*, 49:4552 – 4560, 2011.